JOURNAL OF GEOPHYSICAL RESEARCH, VOL. 104, NO. D16, PAGES 19,443-19,461, AUGUST 27, 1999

Project to Intercompare Regional Climate Simulations (PIRCS): Description and initial results

Eugene S. Takle,[1,2,3] William J. Gutowski Jr.,[1,2] Raymond W. Arritt,[2] Zaitao Pan,[2] Christopher J. Anderson,[2] Renato Ramos da Silva,[2] Daniel Caya[4], Shyh-Chin Chen[5], F. Giorgi,[6] Jens Hesselbjerg Christensen,[7] Song-You Hong,[8] Hann-Ming Henry Juang,[8] Jack Katzfey,[9] William M. Lapenta,[10] Rene Laprise,[4] Glen E. Liston,[11] Philippe Lopez,[7] John McGregor,[9] Roger A. Pielke Sr.,[11] and John O. Roads[5]

Abstract. The first simulation experiment and output archives of the Project to Intercompare Regional Climate Simulations (PIRCS) is described. Initial results from simulations of the summer 1988 drought over the central United States indicate that limited-area models forced by large-scale information at the lateral boundaries reproduce bulk temporal and spatial characteristics of meteorological fields. In particular, the 500 hPa height field time average and temporal variability are generally well simulated by all participating models. Model simulations of precipitation episodes vary depending on the scale of the dynamical forcing. Organized synoptic-scale precipitation systems are simulated deterministically in that precipitation occurs at close to the same time and location as observed (although amounts may vary from observations). Episodes of mesoscale and convective precipitation are represented in a more stochastic sense, with less precise agreement in temporal and spatial patterns. Simulated surface energy fluxes show broad similarity with the First International Satellite Land Surface Climatology Project (ISLSCP) Field Experiment (FIFE) observations in their temporal evolution and time average diurnal cycle. Intermodel differences in midday Bowen ratio tend to be closely associated with precipitation differences. Differences in daily maximum temperatures also are linked to Bowen ratio differences, indicating strong local, surface influence on this field. Although some models have bias with respect to FIFE observations, all tend to reproduce the synoptic variability of observed daily maximum and minimum temperatures. Results also reveal the advantage of an intercomparison in exposing common tendencies of models despite their differences in convective and surface parameterizations and different methods of assimilating lateral boundary conditions.

1. Introduction

Contemporary global climate models have typical resolutions of the order of hundreds of kilometers or larger [*Phillips*, 1995], in part due to computational constraints. Although this has been adequate for many purposes, it is not sufficient for resolving landscape regions that are important to human activities such as agricultural zones and watersheds of subcontinental size. Such resolution also is insufficient for simulating regional circulations that may interact with the landscape and influence local climate. Because simulating climate variability in subcontinental regions is important for understanding human impacts of potential climate change, much attention has been devoted in recent years to climate simulation using atmospheric mesoscale models [*Giorgi and Mearns*, 1991; *McGregor*, 1997] driven by output from a coarser resolution global model or, for test purposes, an atmospheric analysis. The limited-area domain of such mesoscale models allows simulations of months or even years at resolutions of just a few tens of kilometers using current computing resources.

The importance of regional climate change prompts a need to understand the capabilities and limitations of using atmospheric mesoscale models to simulate climate. Furthermore, steady improvements in computing power imply that global climate eventually will be simulated routinely at mesoscale resolution. Analysis and interpretation of climate simulations by limited-area mesoscale models will help pave the way for interpreting results of global simulations at these resolutions. Numerous publications have documented capabilities of a variety of these models to simulate climate adequately in several regions [*Giorgi and Mearns*, 1991; *McGregor*, 1997]. Despite these successes, the overall strengths and weaknesses of this approach to climate simulation have been difficult to assess because the disparate applications reviewed by *Giorgi and Mearns* [1991] and *McGregor* [1997] lack a common framework.

The Project to Intercompare Regional Climate Simulations (PIRCS) was developed to provide a common simulation

[1] Department of Geological and Atmospheric Sciences, Iowa State University, Ames.
[2] Department of Agronomy, Iowa State University, Ames.
[3] International Institute of Theoretical and Applied Physics, Iowa State University, Ames.
[4] Department of Earth Science, University of Quebec at Montreal, Montreal, Canada.
[5] Scripps Institution of Oceanography, La Jolla, California.
[6] Abdus Salam International Centre for Theoretical Physics, Trieste, Italy.
[7] Danish Meteorological Institute, Copenhagen.
[8] National Centers for Environmental Prediction, Camp Springs, Maryland.
[9] Commonwealth Scientific and Industrial Research Organisation, Mordialloc, Australia.
[10] Marshall Space Fight Center, Huntsville, Alabama.
[11] Department of Atmospheric Science, Colorado State University, Fort Collins.

Paper number 1999JD900352.
0148-0227/99/1999JD900352$09.00

framework for evaluating mesoscale models run in climate mode, both versus each other and, more important, versus observations. Beyond evaluating capabilities of this approach to climate simulation, PIRCS also provides a basis for improving mesoscale climate models, both individually and as a group. For this reason, PIRCS has developed with strong community involvement, through a series of workshops [*Takle,* 1995; *Gutowski et al.*, 1998] and additional informal exchanges among participants and advisors [*WMO*, 1996].

This paper describes the motivation and structure for the first PIRCS simulation experiment, including output and observational data sets archived for analysis. We also present some results from the first experiment which illustrate the collective capabilities of the participating models and this approach to climate simulation. Results demonstrate the advantage of an intercomparison in exposing common tendencies of models despite their differences in convective and surface parameterizations and different methods of assimilating lateral boundary conditions.

2. PIRCS Experiment 1

We describe here general features of Experiment 1. Specific technical details can be found at the PIRCS Web site, http://www.pircs.iastate.edu.

2.1. Domain and Period

The simulation domain for Experiment 1 covers the continental United States with a specific focus on the central region (see Figure 1). Summer periods were chosen because large-scale circulation typically is weaker in summer, so local mesoscale circulation might be expected to play a larger role in regional climate. This places a greater challenge on the models to generate regional climate internally without strong external control through lateral boundary conditions. Our simulations cover May 15 to July 15, 1988, a period of extreme drought in the central United States, which minimizes dependence of model results on convective parameterization. Follow-on studies of 1993 (currently in progress) will examine more fully the impacts of widespread convection and offer a contrast to results for 1988. However, the 1988 period offers an experiment in itself to test whether models can reproduce characteristics of an extreme period. A period of only 2 months was chosen to balance limitations in computational and personnel resources for a largely volunteer effort against the need for simulations long enough to capture climatic behavior. Although recent advances in computing hardware have made longer simulations more feasible, there remains substantial benefit from side-by-side simulations performed for the first experiment. The summer of 1998 in the central United States also has been studied numerically by *Giorgi et al.* [1996].

Several factors have guided the choice of simulation domain. A fundamental assumption in PIRCS is that there must be important mesoscale features in the targeted domain for climate simulation by a mesoscale model to give added value to the driving global simulation. The central United States is strongly affected by mesoscale phenomena such as the nocturnal, low-level jet [*Stensrud*, 1996] and mesoscale convective complexes [*Maddox*, 1980; *Fritsch et al.*, 1986]. The central United States also was chosen because it contains a dense climatic observing network whose measurements can be used to assess model performances and has been the site of field campaigns such as the First International Satellite Land Surface Climatology Project (ISLSCP) Field Experiment (FIFE) [*Sellers et al.*, 1992]. The

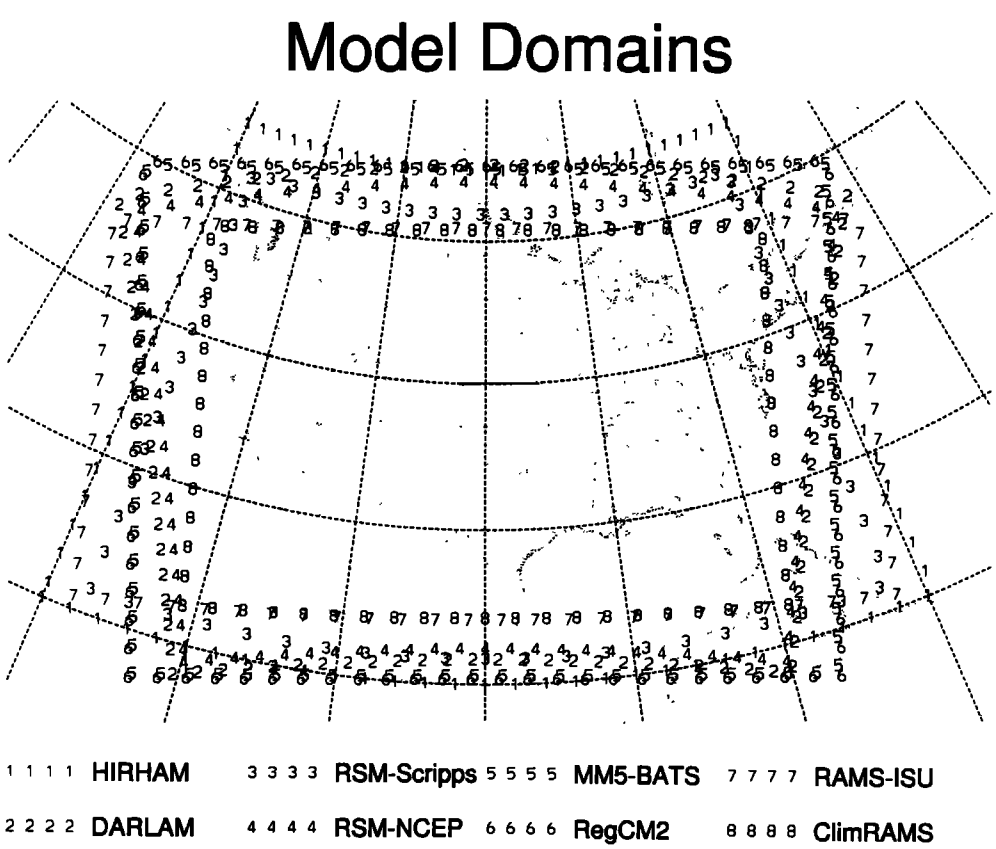

Figure 1. Domains used by models participating in Project to Intercompare Regional Climate Simulations (PIRCS) Experiment 1a.

latter cover only a small part of the simulation domain and only a portion of the simulation period, but they provide information not available from standard climatic networks.

The simulation domain was chosen to minimize as much as possible the presence of mountain ranges near the boundaries, which can interfere with translating coarse-resolution driving data into mesoscale resolution boundary conditions [*Hong and Juang*, 1998]. One outcome of this consideration is that the simulation domain also covers western U.S. mountain ranges, providing an opportunity to simulate and analyze topographic precipitation that will be resolved only crudely in a global climate model. *Seth and Giorgi* [1998] simulated the central United States for 1988 and demonstrated that domains much larger than the area of interest are needed for evaluating sensitivity to internal forcings, one of the purposes of PIRCS. PIRCS models include a variety of grid structures (i.e., some models use rotated latitude-longitude grids, whereas others use polar stereographic or Lambert projections). Domains used by participating models are shown in Figure 1.

Finally, partly for the same reasons as given here, the central United States is the focus region for the Global Energy and Water Experiment Continental International Project (GCIP) [National Academy of Sciences (NAS), 1998]. One goal of GCIP is to improve simulation of climatic water and energy cycles. PIRCS is helping GCIP attain this goal by providing a framework for assessing mesoscale model simulation of these cycles.

2.2. Initial and Boundary Conditions

Atmospheric initial and boundary conditions were extracted from the reanalysis produced by the National Centers for Environmental Prediction (NCEP) and the National Center for Atmospheric Research (NCAR) [*Kalnay et al.*, 1996]. We treated the reanalysis as output from a "perfect" model of the atmosphere for the periods simulated and thus conservatively assumed that differences between model output and observed behavior represent simulation errors due to factors such as construction and ingestion of boundary conditions and internal shortcomings in the models. This assumption is most reasonable for large-scale mass, temperature, and momentum fields and less so for humidity [*Trenberth and Guillemot*, 1995].

Initial and boundary conditions used the finest output resolution available, sigma-layer fields on the T62 Gaussian grid of the data assimilation cycle forecast model. PIRCS scientists at Iowa State University extracted initial and boundary conditions for the mesoscale models by interpolating reanalysis output to a 25 hPa vertical grid spanning 25-1050 hPa and three sets of horizontal grids: 0.5° latitude-longitude grid, 60 km polar stereographic projection, and 52 km Lambert conformal projection. The relatively high lower-boundary pressure of the driving conditions data set was chosen to accommodate mesoscale models in regions where their surface topography is lower, and thus at higher pressure, than the reanalysis topography. Horizontal interpolation was performed to produce driving files matching or nearly matching the standard PIRCS resolution of 60 km. A small degree of additional interpolation was needed to transfer initial and boundary condition files to forms actually ingested by individual models. However, by performing the initial coarse to fine grid interpolation, PIRCS scientists ensured that all models used nearly uniform interpolation of the reanalysis data to mesoscale resolution.

Oceanic portions of the simulation domain used sea surface temperatures (SSTs) derived from the reanalysis SST data set. These were supplemented by direct observations of surface temperature in the Great Lakes and satellite observations of SST in the Gulf of California, where the reanalysis grid gave only coarse resolution. The combined data sets were interpolated to PIRCS grids using a Cressman scheme with three iterations of decreasing radius of influence.

The most problematic initial condition was soil moisture. Over most of the PIRCS domain, this field is not observed regularly, necessitating use of an indirectly estimated soil moisture field. Furthermore, because the spin-up time for soil moisture simulation is probably several weeks or months, any errors in initial soil moisture will persist throughout the simulation. For consistency with atmospheric driving conditions, PIRCS used the soil moisture produced by the surface parameterization of the reanalysis forecast model. Because participating models use a variety of soil layer resolutions, PIRCS supplied a vertically uniform available water fraction, ranging from zero at wilting point to 1 at field capacity. The reanalysis soil moisture is subject to relaxation toward an estimated annual climatology [*Roads et al.*, this issue] and thus must be viewed with caution as an initial condition. The hydrologic extreme of 1988 reduces the uncertainty of initial soil moisture by providing a period when soil in the central United States was very dry. However, individual soil moisture parameterizations can react rather differently to soil moisture near the wilting point, so sensitivity to this initial condition still may exist.

2.3. Output Archive

Anticipated analyses of model output have guided development of the structure of the output archive. A general goal of the archive is to permit analysis of key mesoscale features and of energy and water cycles linked to mesoscale behavior. Therefore most fields are saved at least 4 times daily to allow analysis of diurnal variability. An additional goal has been to have a relatively simple archive to minimize confusion and mistakes in creating it and to promote archive accessibility.

Table 1 lists fields contained in the standard PIRCS archive. Some fields such as precipitation and daily minimum and maximum temperature are included because they are observed at relatively high spatial resolution by climate-observing networks. Others, such as surface fluxes, are included even though they are more sparsely observed because of their key roles in regional energy and water cycles and their usefulness for interpreting how each model develops its climate. Archived output will be available to the general community, although users are required to maintain contact with PIRCS and participating modelers to ensure clear understanding of what models can and cannot do.

2.4. Participating Models

Participation in PIRCS currently is open to all modeling groups willing to perform the simulations and furnish output in the standard format. For this initial report, output is available from eight models. Table 2 gives a summary of key features of participating models.

3. Initial Results

3.1. The 500 hPa Height Field

We used the NCEP reanalysis as a standard for evaluation of the magnitude of the 500 hPa height anomaly. The density of rawinsonde observations over the United States is such that large-scale, upper air fields in the reanalysis are well observed. Time-average 500 hPa heights from the reanalysis for May 15 to July 15, 1988, show that the central United States was dominated by a

Table 1. Data Collected by PIRCS Archive

Interval	Variable Type	Specific Variable
Once	model features	latitude of each point on the horizontal grid used to report model output
		longitude of each point on the horizontal grid used to report model output
		vertical levels used to report model output
		terrain height
		land fraction of each grid cell
Three hourly[a]	surface fluxes	incident solar (shortwave) radiation
		reflected solar (shortwave) radiation
		upward terrestrial (longwave) radiation
		downward terrestrial (longwave) radiation
		sensible heat flux
		latent heat flux (evapotranspiration)
		heat flux from the atmosphere into the model domain below the atmosphere
		convective precipitation
		stable precipitation
		momentum flux into the ground: E-W component (Direction is with respect to the Earth's latitude/ longitude grid.)
		momentum flux into the ground: N-S component (Direction is with respect to the Earth's latitude/ longitude grid.)
	mass	surface pressure
		sea level pressure
		precipitable water (water vapor only)
	temperature	surface air temperature (2 m level)
		skin temperature
Six hourly[b]		temperature
		specific humidity
		zonal (east-west) wind
		meridional (north-south) wind
		geopotential height
		pressure
Daily [c]	2-m air temperature	daily maximum (period: 0000 UTC -0000 UTC)
		time of daily maximum
		daily minimum (period: 0000 UTC - 0000 UTC)
		time of daily minimum
	Soil moisture	total amount of water in the soil column at 1200 UTC
	Runoff	accumulation over prior 24 hours (period: 0000 UTC – 0000 UTC)

[a]Model output reported at 0000,0003,0600 ..., 2100 UTC. For fluxes the output is a 3-hour accumulation (e.g., output at 1200 UTC is accumulated from 0900 UTC- 12 UTC). For mass and temperature, output is the value at the reporting time. Values are reported on the horizontal grid of the participating model.

[b] Atmospheric output sampled at 0000,0600, 1200, and 1800 UTC. Output reported on the three-dimensional grid of the participating model.

[c] Output reported on the horizontal grid of the participating model.

large-scale ridge (Figure 2) whose height anomalies departed from climatology by up to 30 m. For detailed discussion of large-scale features of the 1988 drought, see *Atlas et al.* [1993] and *Trenberth and Guillemot* [1996].

We compared the 500 hPa height field for each model to that for the reanalysis using two statistics, the bias and the root-mean-square deviation (RMSD). Bias is simply the arithmetic mean of the difference between model-predicted and reanalysis 500 hPa height. Bias reflects systematic overpredictions or underpredictions, while transient positive and negative errors may cancel. Conversely, while errors of opposite sign will not cancel in the RMSD, information on the sign of the error is lost. Bias and RMSD were computed at all grid points from output archived every 6 hours. A rough scale for evaluating magnitudes of bias and RMSD is given by the NCEP 500 hPa temporal standard deviation, which was 60-100 m across much of the United States.

Table 2. Models Participating in PIRCS Experiment 1a

Model	Investigator	Grid	Levels	Dynamics	Convection Scheme	Lateral Boundary Condition	Reference
RSM-NCEP	Hong	PS	28	HYD	Grell	EXP/10	*Juang et al.* [1997]
RSM-Scripps	Roads, Chen	MER	28	HYD	A-S	EXP/10	*Juang and Kanamitsu* [1994]
MM5	Lapenta	LC	32	NON	Grell	LIN/4	*Grell et al.* [1993], *Lakhtakia* and *Warner* [1994]
RegCM2	Pan	LC	14	HYD	Grell	EXP/10	*Giorgi et al.* [1993a,b], *Giorgi et al.*[1996]
DARLAM	McGregor,Katzfey	PS	18	HYD	Modified A-S	EXP/9	*McGregor et al.* [1993], *McGregor* and *Walsh* [1994]
HIRHAM4	Christensen, Lopez	MER	19	HYD	MF	EXP/10	*Christensen et al.* [997]
ClimRAMS	Liston, Pielke	PS	20	NON	K-A	PAR/10	*Pielke et al.* [1992]
ISU RAMS	Silva	PS	24	NON	K-A	PAR/8	*Pielke et al.* [1992]

Dynamics: HYD, hydrostatic; NON, nonhydrostatic. Horizontal grid types: MER, Mercator (latitude-longitude); PS, polar stereographic; LC, Lambert conformal. Convection scheme: *AS, Arakawa* and *Schubert* [1974]; *Grell* [1993] and *Grell et al.* [1993]; MF, mass flux scheme following *Tiedtke* [1989]; CA, convective adjustment; *KA, Kuo* [1974]. Lateral BC: weighting function used blending large-scale and internal tendencies (LIN, linear decrease toward center of domain; EXP, exponential decrease; PAR, parabolic decrease) and number of grid points in the blending region.

The time-average RMSD for all participating models except ISU-RAMS shows a rather similar pattern in which there is a broad RMSD maximum across the central to southern United States (Figure 3). For DARLAM, HIRHAM, and ClimRAMS the region of maximum RMSD generally coincides with a broad maximum of bias. We see two possible interpretations (which are not mutually exclusive) for such results. First, the RMSD maxima may be attributable to systematic error in the prediction of the amplitude of the 500 hPa ridge that prevailed over North America during the period. June 1988 monthly average height anomalies versus 1979 – 1988 reanalysis climatology range from near zero in south central United States to over 100 m in north central United States (not shown).

Second, the error may be largest in this region because it is relatively far removed from the boundaries where information from the reanalysis is continually inserted, so that the RMSD pattern may not reflect the ability of the model to predict a particular atmospheric feature. The latter seems to be especially the case for MM5-BATS, in which the RMSD is small near the lateral boundaries and gradually increases toward the interior of the domain. RegCM2 shows two spatial maxima of RMSD, one in the lee of the Rocky Mountains and the other across the east central United States. The former coincides with a positive maximum in bias (perhaps suggesting a systematic error in prediction of lee cyclones or other orographic influences on the dynamics), and the latter corresponds to a broad region of negative bias.

The temporal trend of the spatially averaged RMSD (Figure 4) shows that most models exhibit a base level of RMSD around 10-20 m with occasional episodes of higher values. There was a period about 5 to 10 days after the start of the simulation (Julian days 140-145, May 20-25) when the RMSD was relatively large for most models. During this time a strong 500-hPa closed low slowly migrated across the United States. June 1988 monthly average height anomalies versus 1980-1995 reanalysis climatology (not shown) range from near zero in south central

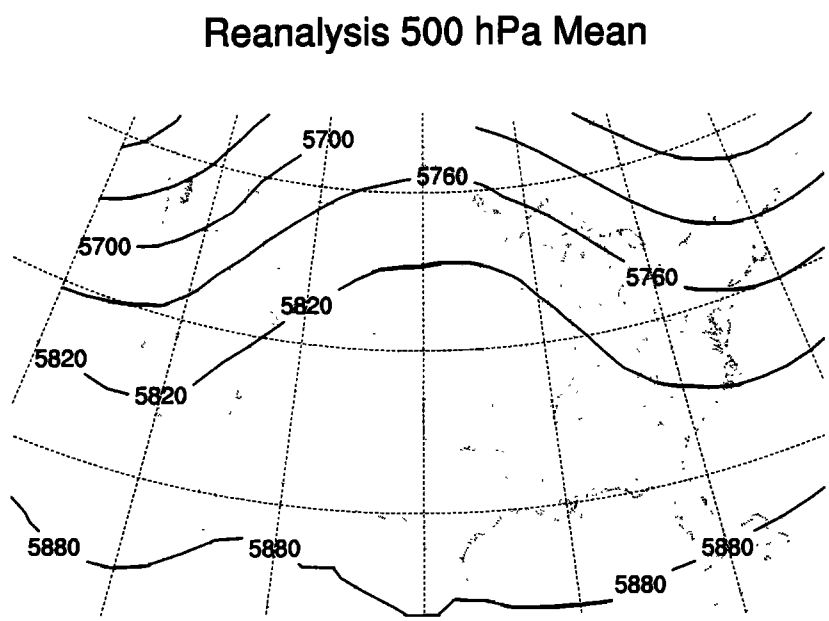

Figure 2. Time-average 500 hPa height field (m) for May 15 to July 15, 1988, from the National Centers for Environmental Prediction/National Center for Atmospheric Research (NCEP/NCAR) reanalysis.

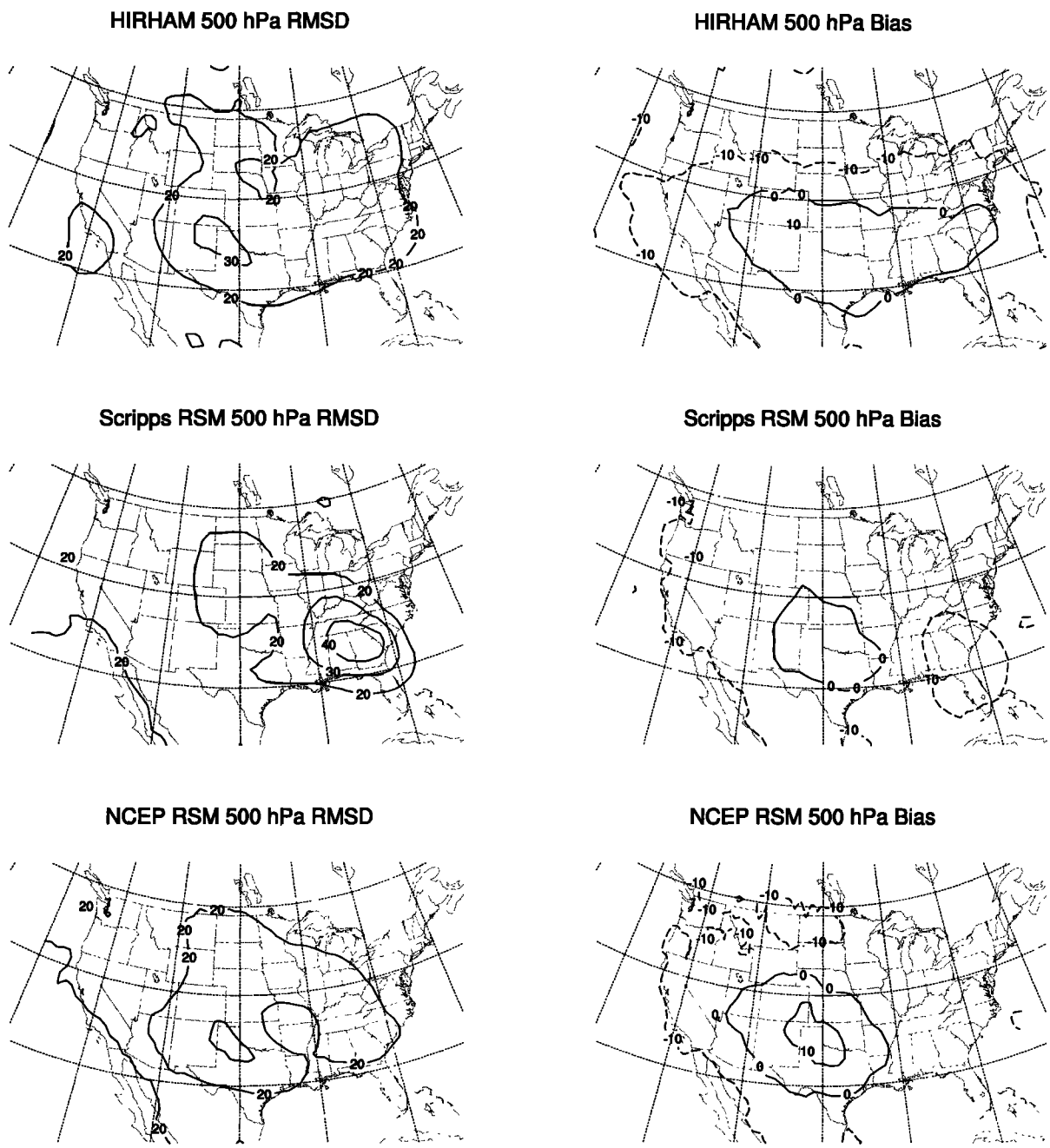

Figure 3. Time-average root-mean-square deviation (RMSD) (left) and bias (right) of model predicted 500 hPa heights (m) compared with the NCEP/NCAR reanalysis.

United States to over 100 m in north central United States. MM5-BATS had a second period of increasing RMSD during Julian days 146-157, when a strong cutoff low persisted over the south central United States. When the cutoff low filled, the RMSD decreased dramatically for MM5-BATS. For Julian days 158-186 the RMSD was near minimum for all models. This was a period characterized by the gradual breakdown, partial redevelopment, and continued breakdown of an intense middle and upper tropospheric ridge over the central United States. Near the end of the simulation there was an episode when RMSD increased for RegCM2 and DARLAM. The increased RMSD corresponded to the development and migration of a weak trough across the central United States. In a broad sense the models appear to handle development and breakdown of large-scale ridges well but evolution of short-wavelength lows somewhat less well; however, there are substantial variations from model to model and from case to case.

Comparison of the standard deviation of model 500 hPa heights with the corresponding statistic from the reanalysis (Figure 5) shows how well model storm tracks match those in the reanalysis. The reanalysis shows maxima of 500 hPa standard deviation in the northwestern and northeastern United States, with a minimum in the central United States implying that storm tracks are blocked. All models reflect this general pattern quite closely

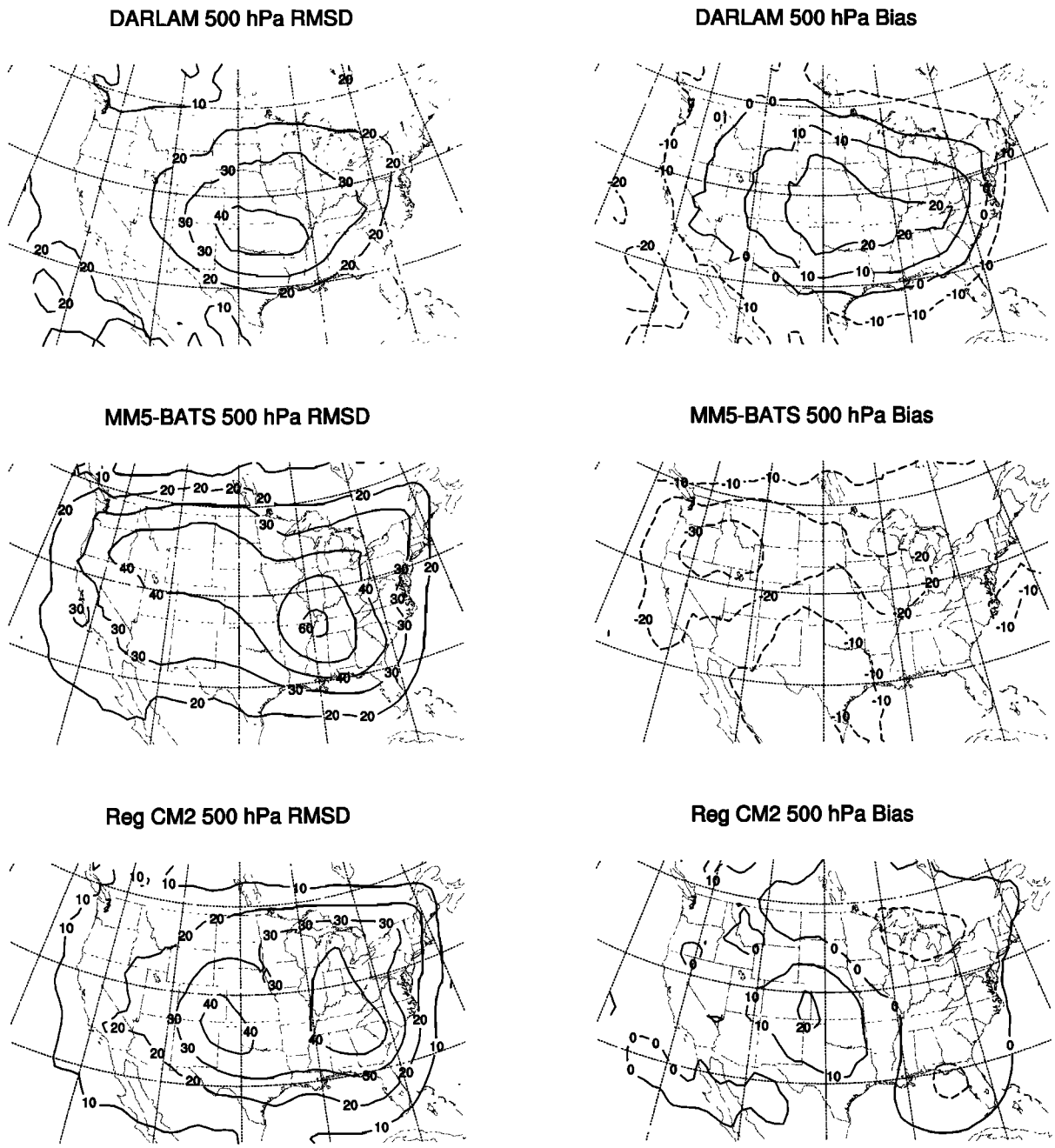

Figure 3. (continued)

(not shown), suggesting that in general the reanalysis data applied in the boundary conditions are adequate for the models to represent the variability of the upper level height fields.

3.2. Precipitation

Evaluation of simulated precipitation uses daily observations from the U.S. Cooperative Observing Network [*National Climatic Data* Center (*NCDC*), 1990] which have been interpolated to a 0.5° latitude-longitude grid using a five-iteration Cressman scheme in which the radius of influence starts at 900 km and is halved in successive iterations. Note that the Cooperative Network data exist only for the United States and thus provides no information on rainfall over Canada, Mexico, or the oceans. Model output was produced on the same grid using bilinear interpolation from each model reporting grid.

Simulated time-average precipitation in the United States is generally closer to 1988 observations (Figure 6) than the climatological mean (not shown). Model bias (Figure 7) is relatively small for some general features of the observed precipitation, such as the wet Pacific Northwest, dry southwestern United States, and wet Atlantic/Appalachian region. For the central United States, the models capture the strong departure from climatological average, but composite model bias (all models in Figure 7) shows difficulty in capturing both the relatively large precipitation in Texas and the region of smallest precipitation in Illinois and Indiana during the 1988 drought. The composite bias tends to appear in all models to varying degrees,

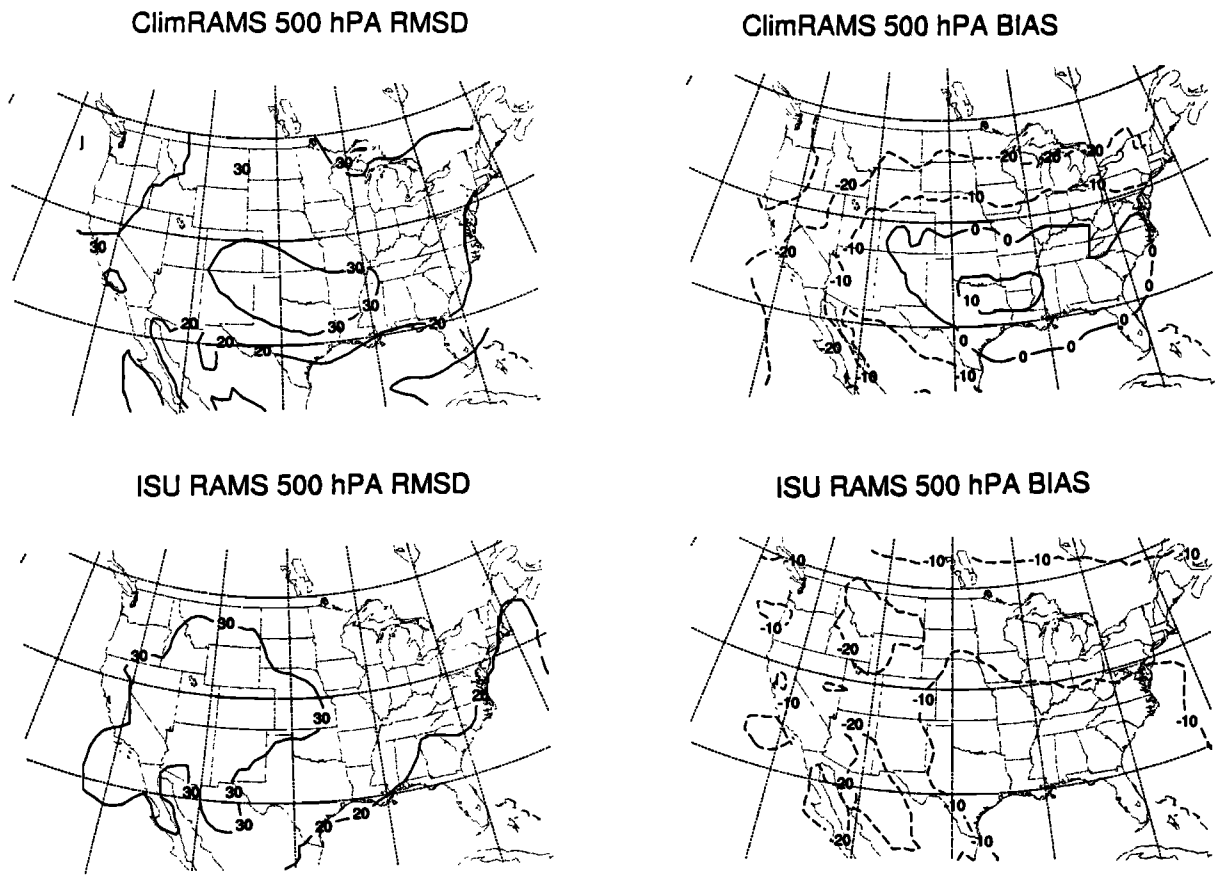

Figure 3. (continued)

indicating a difficulty in simulating precipitation processes for the central United States that applies to all models.

Further analysis of predicted precipitation focuses on a portion of the Upper Mississippi River basin (37°N-47°N, 89°W-99°W) which is well resolved by PIRCS models (about 400 grid points) but poorly resolved by Global Climate Model (GCMs) or reanalysis data. Table 3 summarizes weather patterns that formed central U.S. climate during May-July 1988. Two prominent episodes occurred during this period: (1) Julian days 139-158, dominated by large-scale, synoptic systems and (2) Julian days 164-178, primarily local variability, especially in precipitation.

During the former episode, external boundary conditions are expected to exert substantial influence through their guidance of large-scale flow. During the latter episode, external forcing is expected to be weak, with much if not most of the simulated precipitation resulting from quasi-random convection.

Although the models differ in precipitation magnitudes, they do capture the frequency of synoptically forced precipitation (Figure 8), particularly for the four precipitation events during the period dominated by large-scale, synoptic systems (Julian days 139-158). Equally important for hydrologic considerations, the models also capture dry periods with reasonable fidelity during this period. Evidently, all models effectively ingest influences of large-scale, lateral boundary forcing on precipitation. For Julian days 164 - 178, small but frequent amounts of precipitation are observed, with no clearly definable precipitation events. The

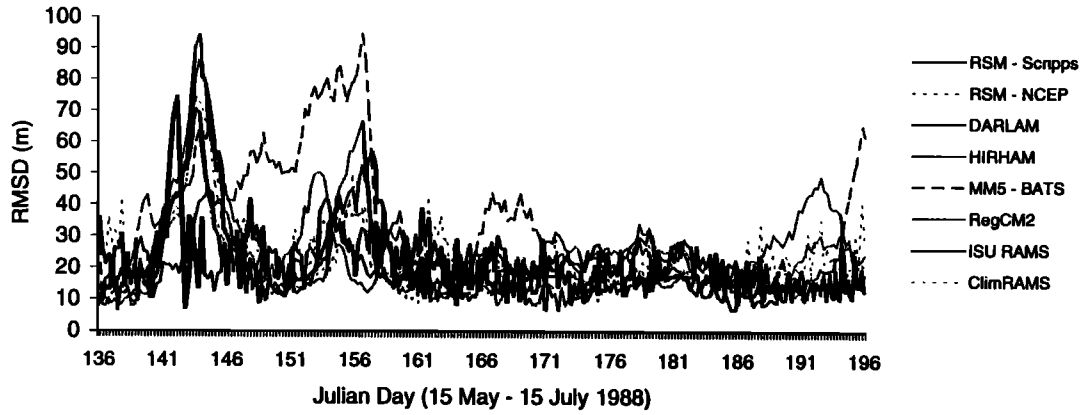

Figure 4. Time series of spatially averaged RMSD of 500 hPa heights (m).

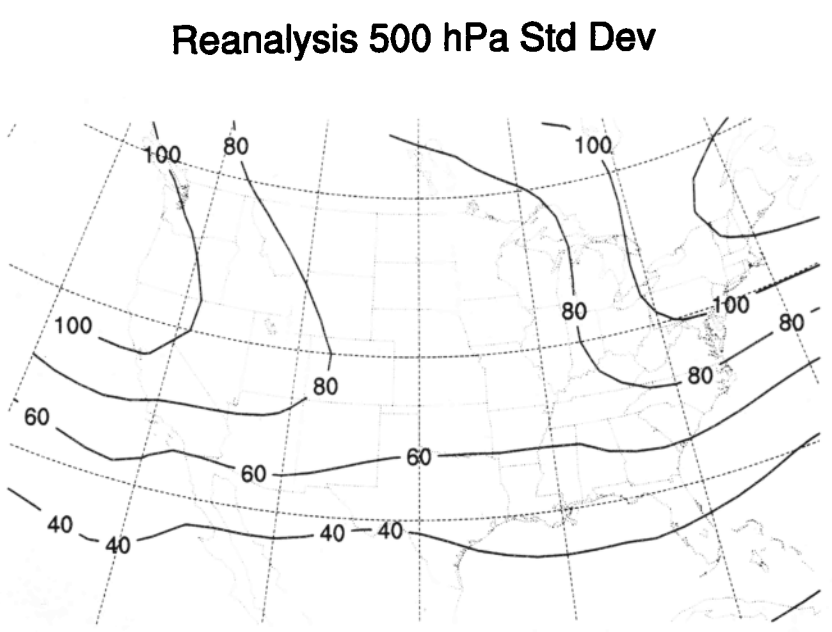

Figure 5. Standard deviation of 500 hPa heights (m) for May 15 to July 15, 1988, computed from the NCEP/NCAR reanalysis.

models represent this stochastic behavior well, although, again, they differ from each other and the observations in precipitation magnitude.

The isolated precipitation event on Julian day 160 is particularly noteworthy. This was a transient event within an overall dry period created by a strong omega block, during which a well-defined precipitation region (likely a mesoscale convective system) migrated across the evaluation subdomain. This event is particularly revealing because its limited spatial and temporal existence 15 days from model initialization and far from forcing boundaries offers challenges for models to simulate. The models capture the existence of this episode quite well, including its

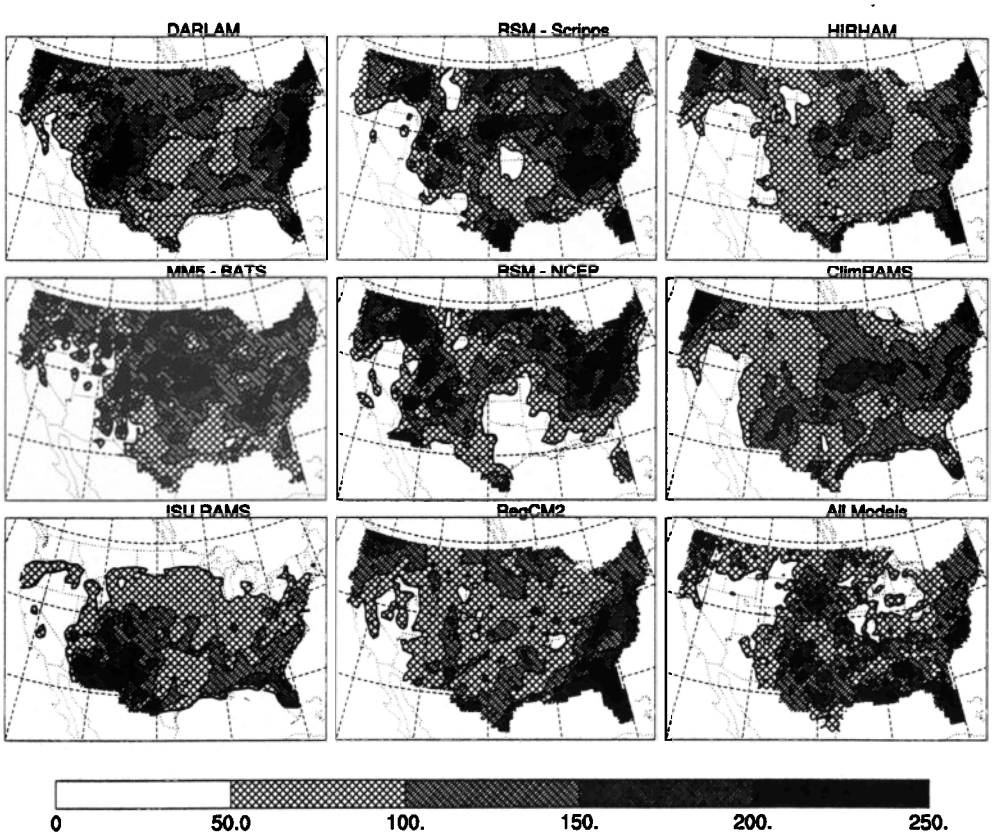

Figure 6. Simulated 60-day accumulated precipitation (mm) for the central United States.

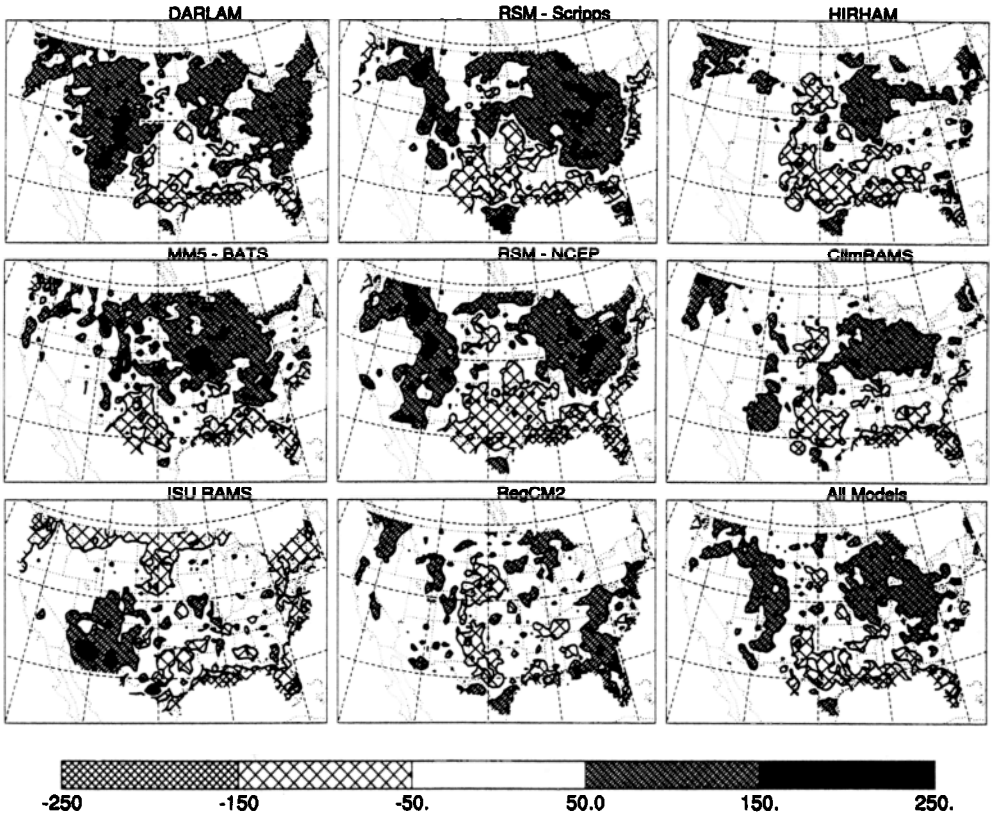

Figure 7. Spatial pattern of model bias (mm) for 60-day total precipitation.

temporal isolation within a generally dry period, although as before, some difficulty is noted for individual models in simulating the correct precipitation amount.

Giorgi [1990] and *Giorgi and Mearns* [1991] report that their regional model run in climate mode was capable of transporting remotely introduced water vapor and producing precipitation that on average matches observed spatial and temporal patterns reasonably well. Our results suggest that this capability is shown more generally by regional models having a wide variety of convective and surface parameterizations and different methods of assimilating lateral boundary conditions.

While the primary focus of PIRCS is the central United States, it is of interest to evaluate model performance for other portions of the domain. Here we briefly examine the temporal trends of area-average precipitation in three latitude-longitude rectangles corresponding to three regions within the domain of most PIRCS

Table 3. Weather Patterns During PIRCS Experiment 1a (May 15 to July 15, 1988)

Julian Day	Date	Synoptic Pattern
137-144	May 16-23	Well-organized synoptic precipitation with centers on both coasts followed by large precipitation regions migrating across United States; peak precipitation from stationary low in central Missouri giving heavy precipitation through central states
145-146	May 24-25	Dry period; rain moves to eastern United States
147-150	May 26-29	Persistent high in southern United States with light discontiguous precipitation in northern U. S. to Canadian border
151-155	May 30 – June 3	Closed 500 hPa low moves across United States, exiting Gulf coast; large organized precipitation patterns
156-159	June 4-7	High dominates United States, very little precipitation
160	June 8	Brief breakdown of high in eastern and southeastern United States, with brief period of precipitation
161-163	June 9-11	Reestablishment of high over whole United States, little precipitation
164-166	June 12-14	Brief, moderate precipitation central United States into Canada.
167-180	June 15-28	500 hPa jet zonal at Canadian border; high across lower United States, very spotty (mesoscale) precipitation patterns dominated by mesoscale processes
181-182	June 29–30	Transition to omega block with more organized precipitation; weak high in Gulf supports LLJ, mesoscale precipitation over broad area of central United States
183	July 1	Transition to weak and spotty precipitation
184-186	July 2-4	Return to dominance by high in southern United States; spotty precipitation
187-190	July 5-8	Scattered areas of light precipitation
191-196	July 9-14	Weakened high, return to organized precipitation

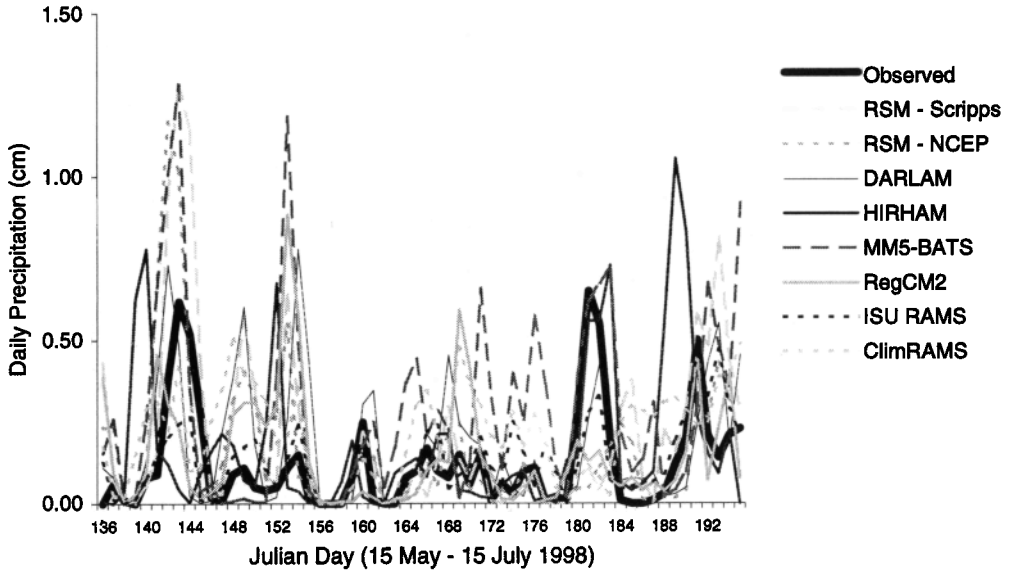

Figure 8. Time series of daily total precipitation (cm) over a portion of the Upper Mississippi River basin (37°-47°N, 89°-99°W).

models: (1) the Pacific Northwest; (2) a portion of the southeastern United States; and (3) the southwest monsoon region as defined by *Higgins et al.* [1997] (see Figure 9 for locations of these regions). The area-average observed precipitation was computed by equal-weighted averaging of all points in the 0.5° precipitation analysis lying within the specified latitude-longitude rectangle. A similar procedure was used for computing area-average precipitation for each of the models; that is, we computed equal-weighted averages of the precipitation for model grid points contained within each region. No attempt was made to adjust observed precipitation for gage undercatch or for station representativeness in regions of irregular terrain.

All models capture the general trend of precipitation in the Pacific Northwest (Figure 10a). (Results for ISU-RAMS and ClimRAMS are not shown for this region, since it lies partially within the lateral boundary zones of the RAMS grids.) For most models the temporal trend of precipitation is well represented, but precipitation amounts are overpredicted. It is noteworthy that most models show a nearly constant positive bias in precipitation compared with the observed area-average trend. This systematic nature of the model error suggests that impacts studies for this region could employ regional climate model output using a MOS-like approach in which the predicted precipitation is statistically calibrated against the observed precipitation.

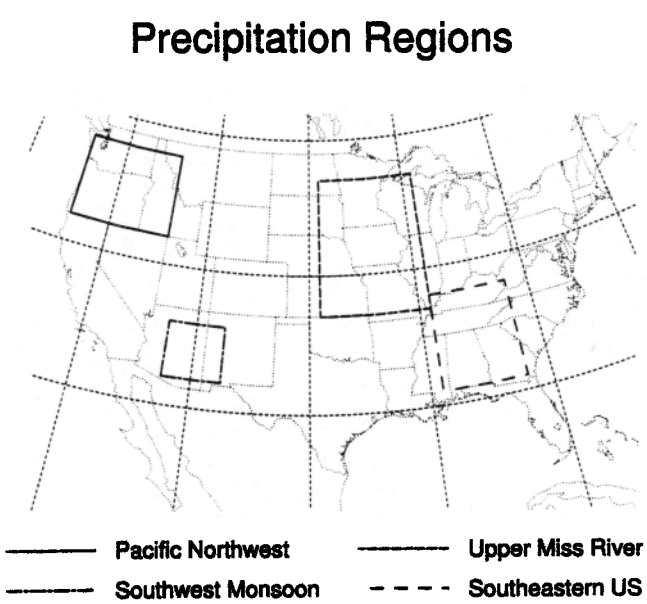

Figure 9. Locations of regions used for analysis of temporal trends of area-averaged precipitation.

For the southeastern United States, most models track the observed precipitation trend, though not so closely as for the Pacific Northwest (Figure 10b). We again find a tendency for most participating models to overpredict precipitation amounts. This does not take the form of a constant bias but also reflects a tendency for some models to produce precipitation during observed dry spells.

Precipitation in the southwest U. S. box was strongly related to the development of a vertically stacked low over Baja California about June 18. Prior to this development, low-level moisture was limited over Arizona and New Mexico, so despite the passage of a number of upper level disturbances, very little rain was generated. Upper level disturbances were much less frequent, while the Baja low was established as well as after its demise. Much of the accumulated rain fell during this time because events were frequent and daily rain rates were very high. Peaks in the time series correspond to the passage of upper level systems.

Precipitation in the southwestern United States is of interest in its own right and also because it reflects the dynamics of the North American monsoon system (NAMS), which has important influences on dynamics and precipitation over our central U. S. focus region. As tabulated by *Higgins et al.* [1997], onset of the NAMS occurred in 1988 around June 24 (Julian day 176). While all models show a noticeable increase in precipitation beginning around this date, there are substantial model-to-model differences (Figure 10c). A few models show only a modest increase in precipitation rates after monsoon onset. Others show an exaggerated signal with near-zero precipitation before monsoon onset and a rapid increase in precipitation afterward.

As discussed by *Barlow et al.* [1998], the NAMS is produced by the combined influences of large-scale circulation patterns and more localized diabatic heating. The former presumably should

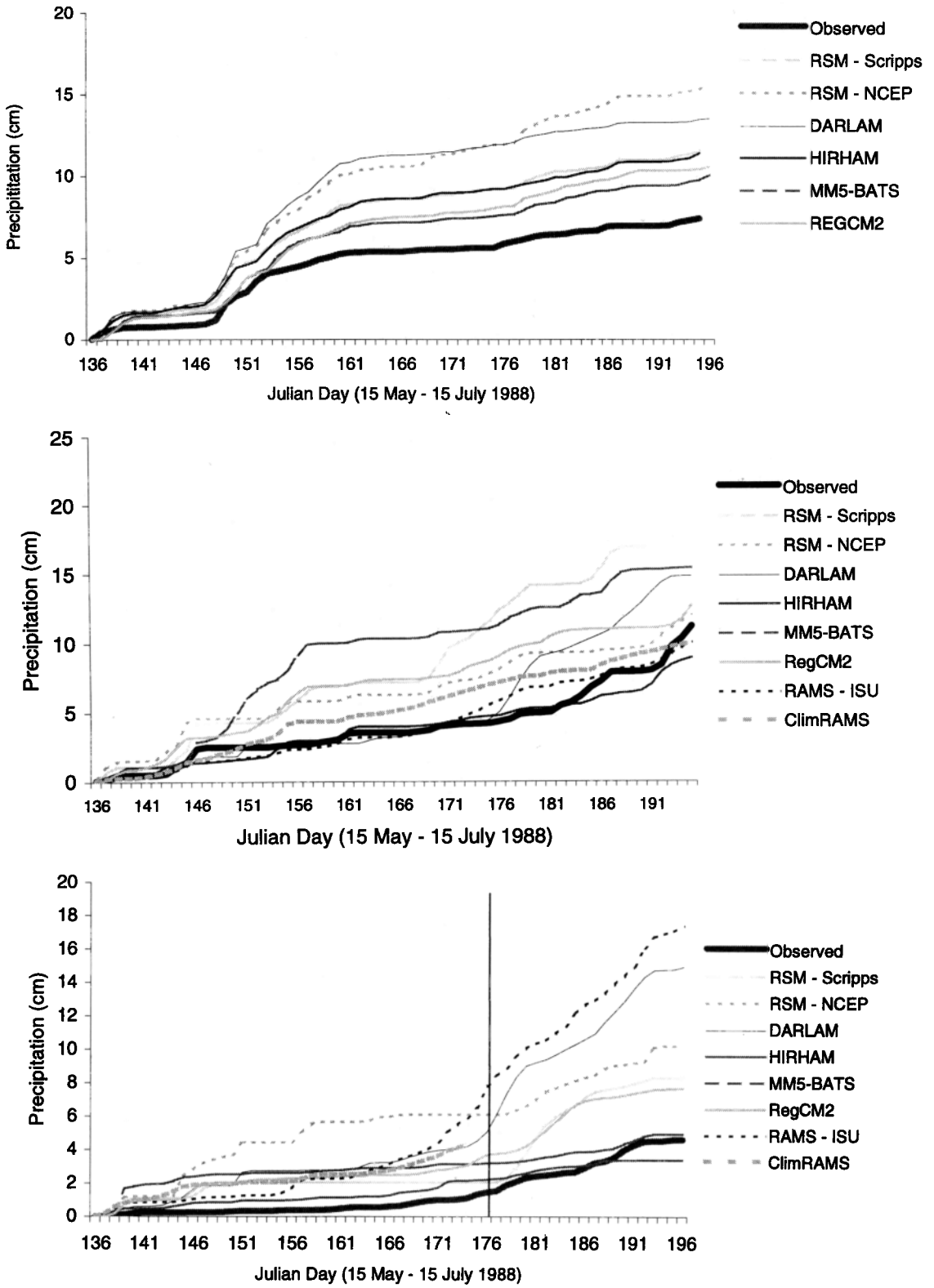

Figure 10. Temporal trend of area-averaged accumulated precipitation (cm) for (a) the Pacific Northwest, (b) Southeast United States, and (c) southwest monsoon region.

be included in the reanalysis-derived lateral boundary conditions, though the relative lack of observations over Mexico and especially the adjacent oceans must be kept in mind. The latter would be strongly affected by model physics, including surface fluxes of sensible and latent heat as well as upper level heating produced by the model convective parameterizations. Diabatic heating over the Mexican plateau, which is only partially included in the model domains, is thought to be an especially important influence on the upper level height patterns that produce the monsoon. (It is worth pointing out that partly for the reasons discussed here, the NCEP/NCAR reanalysis and the European Center for Medium Range Weather Forecasting (ECMWF)

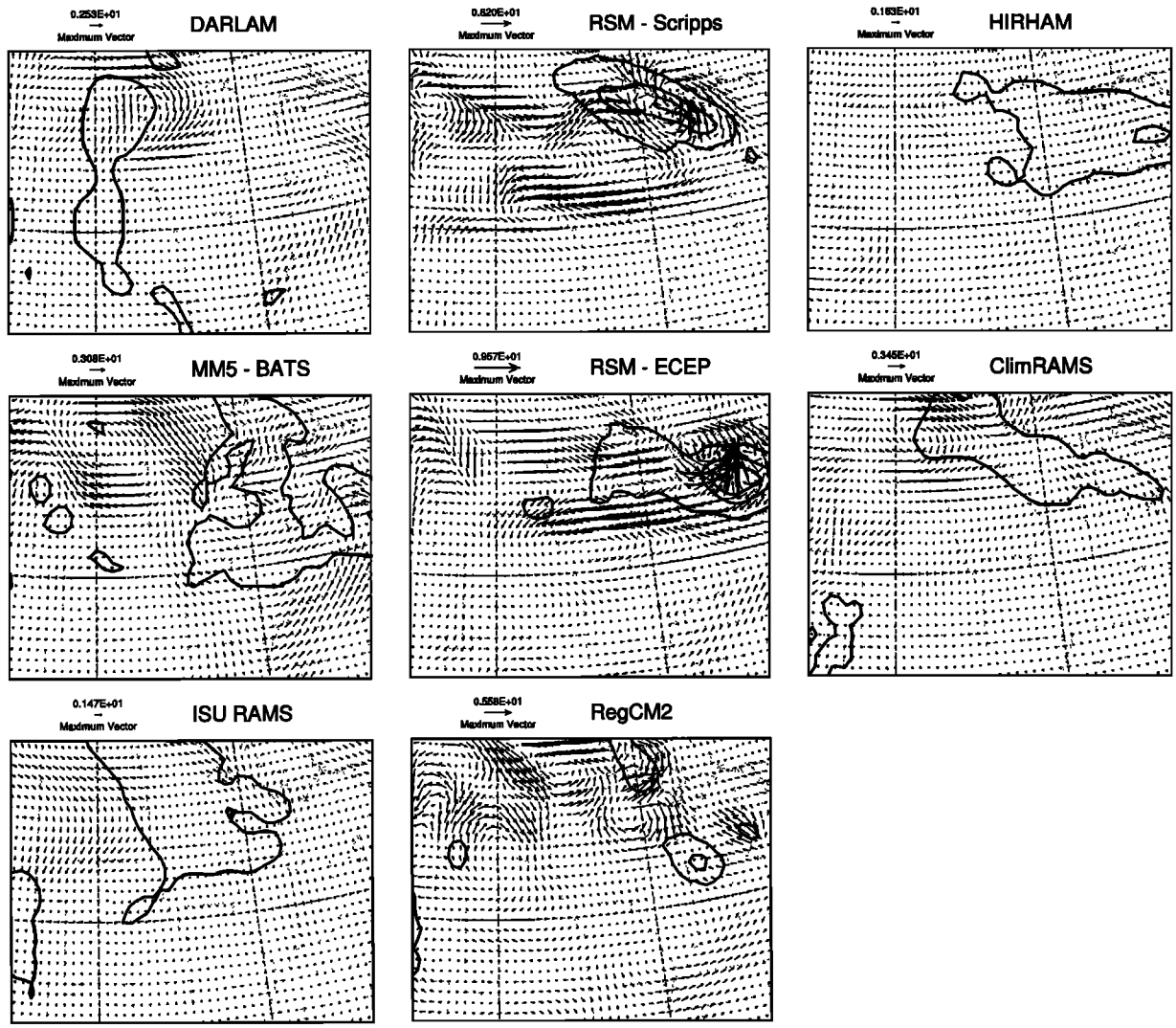

Figure 11. Mesoscale departure winds (m s^{-1}) at 600 hPa over the central United States within 6 hours of 0600 UTC on day 160. Contours give 6 hour precipitation totals of 1, 10, and 20 mm.

reanalysis differ in their representation of the NAMS [*Barlow et al.* 1998].) This consideration suggests that it may be useful to perform a sensitivity experiment that would evaluate the need to include the Mexican plateau within the model domain in order to better depict the NAMS and its effect on summertime climate over the central United States.

3.3. Mesoscale Circulation

We used a mesoscale filter defined by *Giorgi et al.* [1993b] to evaluate localized features of the flow fields produced by individual models. Under this procedure we calculate a local spatially averaged wind vector as the mean of the 9 x 9 point box centered on the local point. This value is subtracted from the model wind vector calculated for the local point to give the local mesoscale departure wind vector, which is plotted for each model in Figure 11. Day 160 offers an opportunity to observe the flow features connected with an isolated (in both space and time) precipitation event. Figure 11 gives the mesoscale departure winds at 600 hPa over the central United States within 6 hours of 0600 UTC on day 160. Some models have accelerated or delayed passage of this event, so for each model, we have selected the map time that best represents passage of the system through this part of the domain.

All models show mesoscale activity and precipitation associated with this disturbance north of the Iowa-Missouri border, with relatively tranquil conditions to the south. Most models produce moderate to strong anticyclonic flow near the Dakota–Minnesota border and strong wind shear and precipitation in the vicinity (to the east in most models). Details differ, with the two regional spectral models (RSM-Scripps and RSM-NCEP), RegCM2, and MM5-BATS giving much stronger departure winds. RegCM2 and RSM-Scripps have precipitation regions extending north of central Minnesota (the northern boundary of the central U.S. precipitation box), which may account for their lower contributions to precipitation on day 160 in Figure 8.

3.4. Surface Fluxes

In addition to large-scale lateral forcing, internal spatial patterns of surface energy and water fluxes also can be important aspects of climate patterns. Such fluxes are not observed on a regular basis over most of the PIRCS simulation domain. To

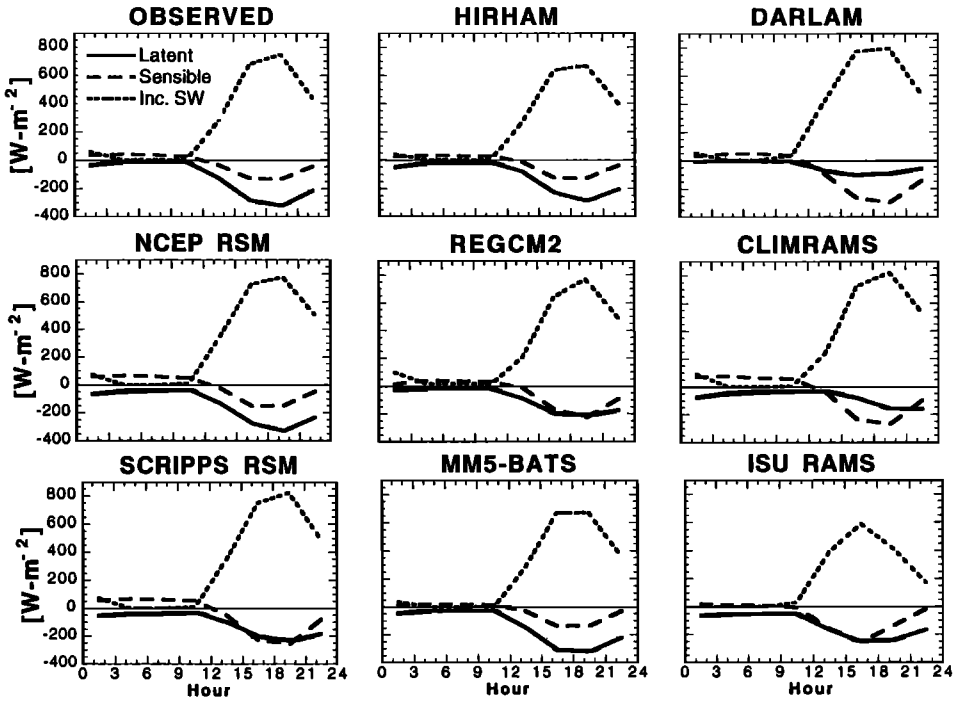

Figure 12. Time-average diurnal cycles of surface latent heat flux, sensible heat flux, and incident shortwave radiation (all given in W m^{-2}) from First ISLSCP Field Experiment (FIFE) observations processed by Betts and Ball [1998] and from each model grid point nearest the FIFE site.

evaluate simulated surface fluxes, we use observed data from the First ISLSCP Field Experiment (FIFE) [*Sellers et al.*, 1992] which were prepared by *Betts and Ball* [1998]. These data have been used previously to evaluate land-atmosphere interaction in large-scale [*Betts et al.*, 1993] and mesoscale [*Betts et al.* 1997] forecast models. In this data set, all available observations over the 15 km x 15 km FIFE region for a field such as surface latent heat flux are averaged together at 30 min intervals. The averaging makes no distinction between instruments, nor does it use any differential weighting such as area weighting. During the PIRCS 1988 period, each interval typically contains reports from several instruments. For each model we extract output from the grid point closest to the 15 km x 15 km FIFE region (39°N, 96.5°W) to compare with FIFE observations. The models use a wide variety of land schemes to simulate surface processes and their interaction with the atmosphere. Most tend to classify the land as some mixture of farm and grassland, though two (RSM-NCEP and RSM-Scripps) use a generic vegetation that is applied to all land points.

Betts and Ball also give standard deviations of reported values at each time step. There are a number of reasons for variations among measurements, such as spatially varying cloud cover [*Smith et al.*, 1992], physical features of the landscape [*Nie et al.*, 1992a], specific vegetation characteristics [*Smith et al.*, 1992], instrumentation differences [*Nie et al.*, 1992b], and measurement error [*Kanemasu et al.*, 1992]. We use the standard deviation among concurrent measurements as a metric for flux-measurement accuracy and plot FIFE instrument average plus and minus the standard deviation.

Figure 12 shows the 60 day average diurnal cycles for three surface fluxes: incident shortwave radiation, latent heat, and sensible heat. Incident shortwave radiation provides the primary energy input to the surface, whereas the latent and sensible heat fluxes combined typically represent most of the net energy received by the atmosphere from the surface. The largest differences among simulations and with respect to observations occur in the Bowen ratio: midday latent heat flux is larger, smaller or approximately equal to the sensible heat flux, depending on the model. FIFE observations give latent heat flux roughly 3 times larger in magnitude than sensible heat flux, but

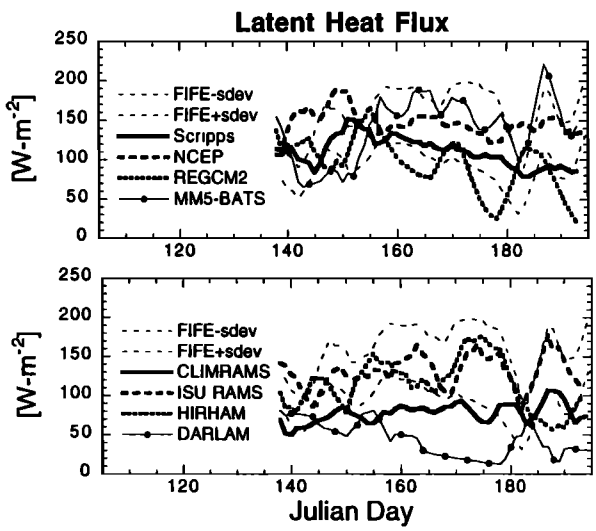

Figure 13. Time series of surface latent heat flux (W m^{-2}) from each model grid point nearest the FIFE site. FIFE curves are each time average over all observing instruments plus or minus the standard deviation among instruments. Models are identified in the key for each panel. All curves have been subjected to a 5 day running average.

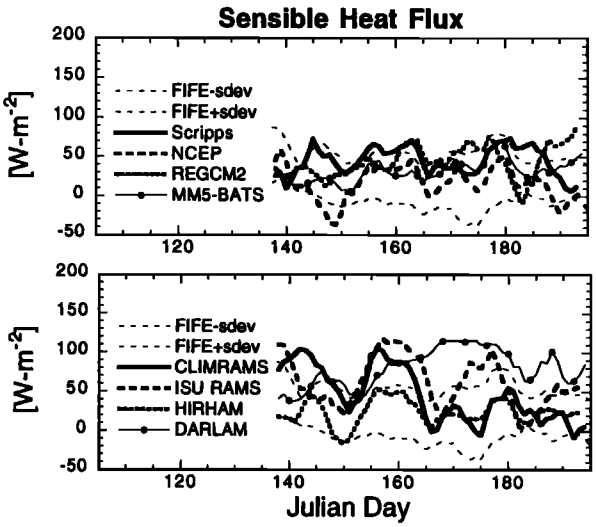

Figure 14. Like Figure 13 but for surface sensible heat flux.

some caution should be exercised in evaluating FIFE sensible and latent heat fluxes for 1988. *Betts and* Ball [1998] note that combined precipitation, evapotranspiration, and soil moisture measurements for 1988 do not give balance in the soil moisture budget. Also, the surface latent heat flux observed for 1988 is as large as observed for 1987, even though the FIFE region experienced an intense drought in 1988. Model results show better agreement for incident solar radiation. Models simulating greater central U.S. precipitation also tend to have smaller insolation maxima, presumably because of greater simulated cloud cover.

Time series of daily surface latent heat flux (Figure 13) and sensible heat flux (Figure 14) show the same relative behavior among models as revealed in their average diurnal cycles. If we accept the FIFE observations as reasonable representations of actual fluxes, despite the cautions above, then most models are simulating these two fluxes fairly well, remembering that these comparisons are effectively for a single point. The models also simulate daily insolation (Figure 15) moderately well, with several roughly reproducing the synoptic variability of the FIFE observations.

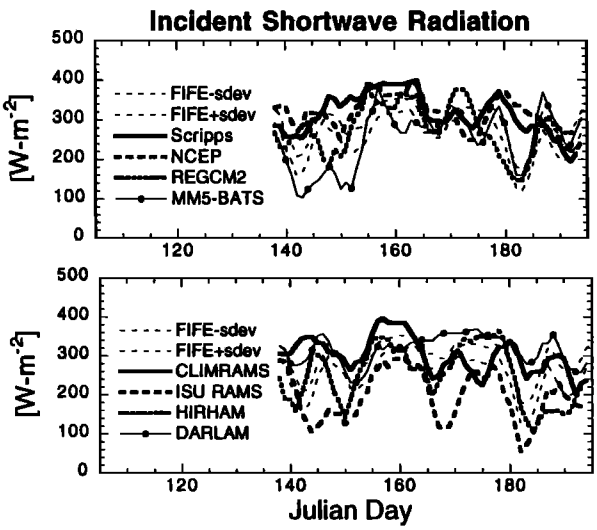

Figure 15. Like Figure 13 but for incident solar radiation.

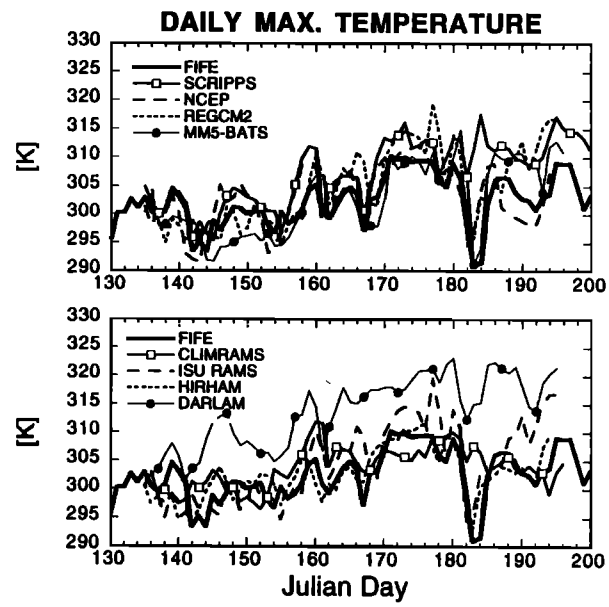

Figure 16. Time series of daily maximum temperature (K) from FIFE observations processed by Betts and Ball [1998] and from each model grid point nearest the FIFE site.

3.5. Daily Minimum and Maximum Temperature

An important outcome of surface-atmosphere interaction and synoptic weather fluctuations is the time variation of daily minimum and maximum temperature. For daily maximum temperature (Figure 16), models tend to follow the observed synoptic variability, though with bias. Most models, for example, captured sharp decreases and increases in temperature around days 142, 167, and 183. Bias in maximum temperature tends to correlate with the model midday, time-average Bowen ratios in Figure 12. Coolest maxima occur for MM5-BATS and HIRHAM, which have the smallest Bowen ratio, whereas DARLAM has the warmest maxima as well as the largest Bowen

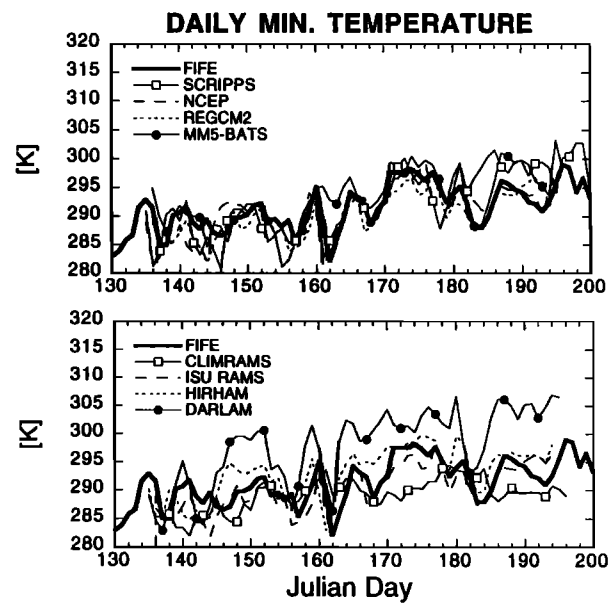

Figure 17. Like Figure 15 but for daily minimum temperature (K).

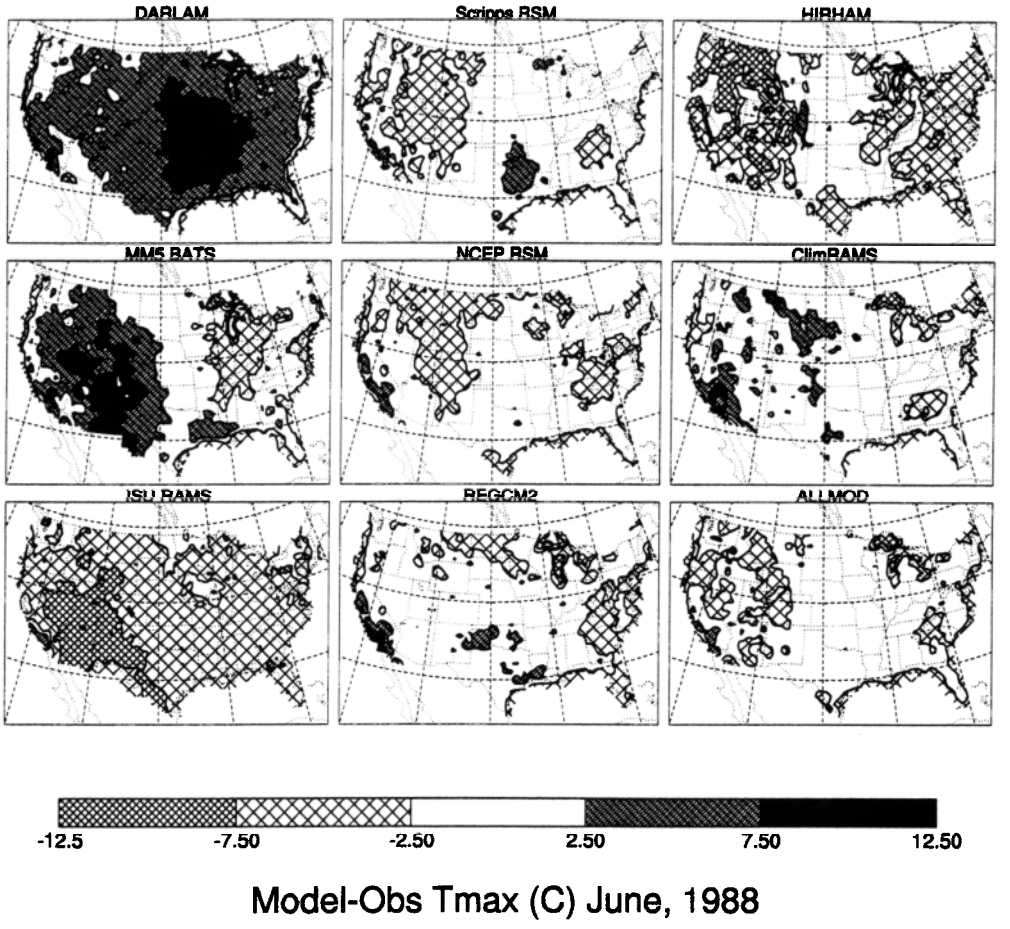

Figure 18. Spatial distribution of model bias for maximum temperature (°C).

ratio. Maximum temperature evolution thus shows evidence of external control by the synoptic flow and local control by surface energy balances.

Daily minimum temperature (Figure 17) also tends to reproduce the synoptic variability of the FIFE observations. Differences between model and observed values are smaller for minimum temperatures than for maximum temperatures. In contrast to maximum temperature, however, model-to-model differences in minimum temperature show less relationship to simulated surface energy balances. Although DARLAM still has the largest positive bias versus FIFE observations, there is otherwise no consistent relationship between Bowen ratio and minimum temperature. This of course is not surprising since minimum temperatures tend to occur at night in the models (as they do in the observations (not shown)), when the surface fluxes shown are weak.

We also compare simulated minimum and maximum temperatures for the United States as a whole, using observations from the U.S. Historical Climate Network [*Peterson and Vose*, 1997]. Because model grid points may have different elevations than nearby observing stations, we transformed all temperatures to a common elevation (sea level) using a 6.5 K/km lapse rate [cf. *Jones et al.* 1995]. We then interpolated observed and simulated temperatures to a common, half-degree grid using the same techniques applied to precipitation fields. The vertical interpolation was not necessary for comparing observations from the relatively flat FIFE region, but it markedly reduced simulation bias in mountainous regions.

In contrast to precipitation the composite bias for maximum temperature (Figure 18) does not indicate common features of all model simulations. In most parts of the United States, both positive and negative model biases appear. No consistent pattern emerges. For minimum temperature (Figure 19) the composite bias indicates a tendency for model temperatures to be too warm in the eastern two thirds of the country and too cool in the southwest, features that appear with varying magnitude in all models. The general behavior is consistent with the FIFE comparison in that the models show more consistency in their daily minimum temperatures than in their daily maximum temperatures.

4. Summary

Limited-area models forced by large-scale information at lateral boundaries are able to reproduce bulk temporal and spatial characteristics of meteorological fields during the 1988 drought. The mean 500 hPa height field is generally well simulated, as is its temporal variability. There is some evidence that model skill varies with the synoptic regime in a common way. Specifically, most models simulate well situations dominated by a ridge or zonal flow as measured by the root-mean-square deviation from the reanalysis data, while periods affected by shortwave lows or troughs (especially cutoff lows) tend to have larger RMSD.

Simulation error of precipitation episodes varies depending on the scale of the relevant dynamical forcing. Organized synoptic-scale precipitation systems are simulated deterministically, in that

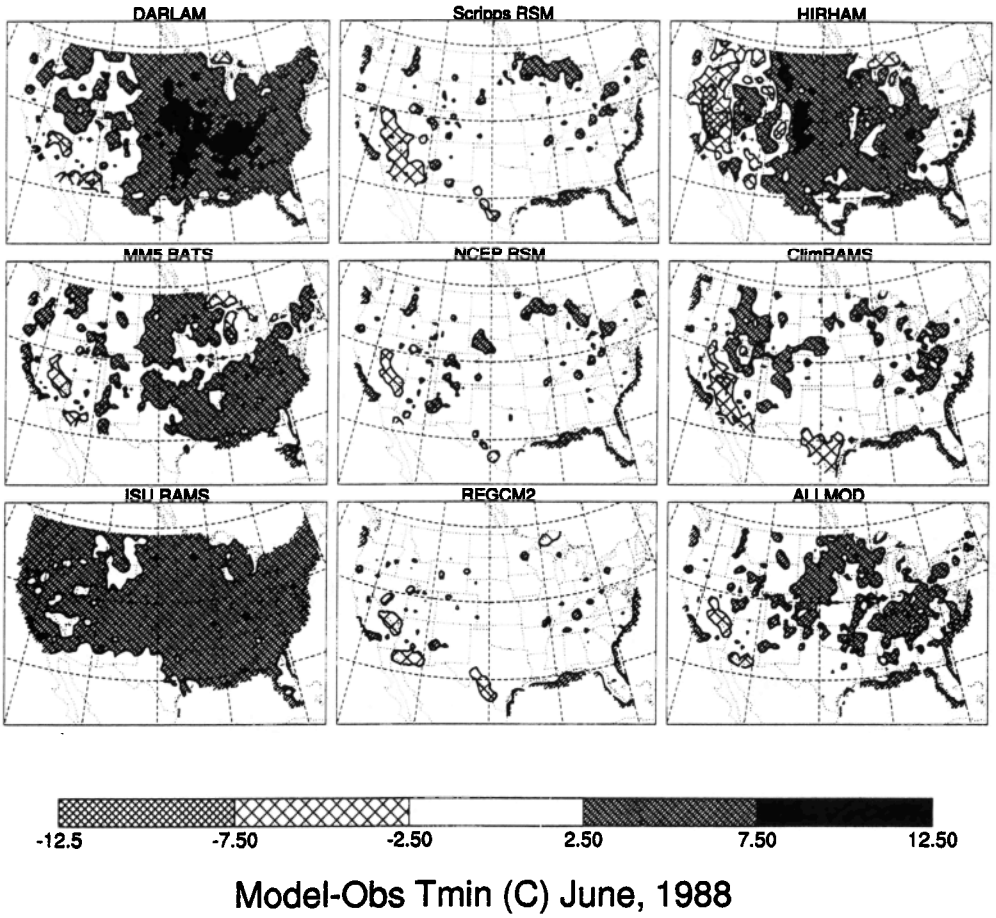

Figure 19. Spatial distribution of model bias for minimum temperature (°C).

precipitation occurs close to the same time and location as observed (though the amounts may vary from the observations). Episodes of mesoscale and convective precipitation are represented in a more stochastic sense: general periods of scattered convective precipitation tend to be captured in the models, though with less precise agreement in temporal and spatial patterns than for the synoptically organized events.

Simulated surface energy fluxes near the FIFE region show broad similarity with FIFE observations in their temporal evolution and time-average diurnal cycle. The largest differences occur in midday Bowen ratio, whose intermodel differences tend to be closely associated with precipitation differences. Differences in daily maximum temperatures also are linked to Bowen ratio differences, indicating a strong local, surface influence on this field. Although some models have bias with respect to FIFE observations, all tend to reproduce the synoptic variability of observed daily maximum and minimum temperatures.

Although there are some common strengths and deficiencies among the models, no single model stands out as best in all comparisons; rather, each model has individual strengths and deficiencies. This feature illustrates the importance of archiving a variety of output fields that can be compared with observations. By providing observed fields and results of all participating models in a common framework, PIRCS allows regional modeling groups an opportunity for identifying weaknesses and prioritizing their development efforts. It also offers a test bed for evaluating new or revised regional climate models.

Several questions can be addressed in more detailed analyses of model results or in additional PIRCS cases, such as the 1993 experiment currently in progress. Examining model ability to predict the Great Plains low-level jet, organized mesoscale convective systems, and the relationship between these two phenomena will allow evaluation of how models link mesoscale dynamics with regional precipitation. Sensitivity studies or ensemble simulations should be performed to evaluate the effect of uncertainties in initial and boundary conditions on the model results. This question is especially important for soil moisture, which as mentioned previously has a rather tenuous observational basis and yet may have substantial influence on predictions. Details of model implementation such as optimal placement of the lateral boundaries [*Jones et al.*, 1995] and improved methods for ingesting large-scale data into limited-area models also deserve attention. Finally, the models must be evaluated for their ability to provide useable information for assessing impacts of climate change in areas such as agriculture, human health, and water resources. Future PIRCS reports will address these issues.

Acknowledgments. The Project to Intercompare Regional Climate Simulations has been supported by funding from the Electric Power Research Institute, the International Institute of Theoretical and Applied Physics, and the Iowa Center for Global and Regional Environmental Research. Additional support for R. W. Arritt and C. J. Anderson was provided under NSF grant ATM-9616728. J. Roads and S. Chen were supported by NOAA grants NA77RJ0453 and NA37GP0372. We gratefully acknowledge Eugenia Kalnay, Linda Mearns, and Andrew Staniforth for advice and support in the design of the project. We also

acknowledge the U.S. National Climatic Data Center (http://www.nndc.noaa.gov) for making available U.S. Cooperative Network data. Three reviewers provided numerous comments that led to substantial improvements in the paper. Scott Kampa and Doug Fils provided computing assistance.

References

Arakawa, A., and W. Schubert, Interaction of a cumulus cloud ensemble with the large-scale environment, I, *J. Atmos. Sci., 31*, 674-701, 1974.

Atlas, R., N. Wolfson, and J. Terry, The effect of SST and soil-moisture anomalies on GLA model simulations of the 1988 U.S. summer drought, *J. Clim., 6*, 2034-2048, 1993.

Barlow, M., S. Nigam, and E. H. Berbery, Evolution of the North American monsoon system, *J. Clim., 11*, 2238-2257, 1998.

Betts, A. K., and J. H. Ball, FIFE surface climate and site-average data set 1987-89, *J. Atmos. Sci., 55*, 1091-1108, 1998.

Betts, A. K., J. H. Ball, and A. C. M. Beljaars, Comparison between the land surface response of the European Centre model and the FIFE-1987 data, *Q. J. R. Meteorol. Soc., 119*, 975-1001, 1993.

Betts, A. K., F. Chen, K. Mitchell, and Z. Janjic, Assessment of land surface and boundary layer models in two operational versions of the Eta Model using FIFE data, *Mon. Weather Rev., 125*, 2896-2916, 1997.

Christensen, J.H., B. Machenhauer, R.G. Jones, C. Schar, P. Ruti, M. Castro, and G. Visconti, Validation of present-day regional climate simulations over Europe: LAM simulations with observed boundary conditions, *Clim. Dyn., 13*, 489 – 506, 1997.

Fritsch, J.M., R.J. Kane, and C.R. Chelius, The contribution of mesoscale convective weather systems to the warm season precipitation in the central United States, *J. Clim. Appl. Meteorol., 25*, 1333-1345, 1986.

Giorgi, F., On the simulation of regional climate using a limited area model nested in a general circulation model, *J. Clim., 3*, 941-963, 1990.

Giorgi, F., and L. Mearns, Approaches to the simulation of regional climate change: A review, *Rev. Geophys., 29*, 191-216, 1991.

Giorgi, F., M. R. Marinucci, G. T. Bates, and G. De Canio, Development of a second-generation regional climate model (RegCM2), I: Boundary-layer and radiative transfer, *Mon. Weather Rev., 121*, 2794-2813, 1993a.

Giorgi, F., M. R. Marinucci, G. T. Bates, and G. De Canio, Development of a second-generation regional climate model (RegCM2), II, Convective processes and assimilation of boundary conditions, *Mon. Weather Rev., 121*, 2814-2832, 1993b.

Giorgi, F., L. O. Mearns, C. Shields, and L. Mayer, A regional model study of the importance of local versus remote controls of the 1988 drought and the 1993 flood over the central United States, *J. Clim., 9*, 1150-1161, 1996.

Grell, G. A., Prognostic evaluation of assumptions used by cumulus parameterizations, *Mon. Weather Rev., 121*, 764-787, 1993.

Grell, G. A., J. Dudhia, and D. R. Stauffer, A description of the fifth-generation Penn State/NCAR mesoscale model (MM5), *NCAR Tech. Note, NCAR/TN-397+STR*, 200 pp., Natl. Cent. for Atmos. Res., Boulder, Colo., 1993.

Gutowski, W. J., E. S. Takle, and R. W. Arritt, Project to Intercompare Regional Climate Simulations, Workshop II, 5-6 June 1997, *Bull. Am. Meteorol. Soc.*, 79(4), 657-659, 1998.

Higgins, R. W., Y. Yao, and X. L. Wang, Influence of the North American monsoon system on the U.S. summer precipitation regime, *J. Clim., 10*, 2600-2622, 1997.

Hong, S.-Y., and H.-M. H. Juang, Orography blending in the lateral boundary of a regional model, *Mon. Weather Rev., 126*, 1714-1718, 1998.

Jones, R. G., J. M. Murphy, and M. Noguer, Simulation of climate change over Europe using a nested regional climate model, I, Assessment of control climate, including sensitivity to location of lateral boundaries, *Q J. R. Meteorol. Soc., 121*, 1413-1449, 1995.

Juang, H.-M. H., and M. Kanamitsu, The NMC nested regional spectral model, *Mon. Weather Rev., 122*, 3-26, 1994.

Juang, H.-M. H., S.-Y. Hong, and M. Kanamitsu, The NCEP regional spectral model: An update, *Bull. Am. Meteorol. Soc., 78*, 2125-2143, 1997.

Kalnay, E., et al., The NCEP/NCAR 40-year reanalysis project, *Bull. Am. Meteorol. Soc., 77*, 437-471, 1996.

Kanemasu, E. T., et al., Surface flux measurements in FIFE: An overview, *J. Geophys. Res., 97*, (D17), 18, 547-18,555, 1992.

Kuo, H.L., Further studies of the parameterization of the effect of cumulus convection on large-scale flow, *J. Atmos. Sci., 31*, 1232-1240, 1974.

Lakhtakia, M. N., and T. T. Warner, A comparison of simple and complex treatments of surface hydrology and thermodynamics suitable for mesoscale atmospheric models, *Mon. Weather Rev., 122*, 880-896, 1994.

Maddox, R. A., Mesoscale convective complexes, *Bull. Am. Meteorol. Soc., 61*, 1374-1387, 1980.

McGregor, J. L., Regional climate modelling, *Meteorol. Atmos. Phys, 63*(1-2), 105-117, 1997.

McGregor, J. L., and K. Walsh, Climate change simulations of Tasmanian precipitation using multiple nesting, *J. Geophys. Res., 99*, 20889-20905, 1994.

McGregor, J. L., K. J. Walsh, and J. J. Katzfey, Nested modelling for regional climate studies, in *Modelling Change in Environmental Systems*, edited by A. J. Jakeman, M. B. Beck, and M. J. McAleer, pp. 367-386, John Wiley, New York, 1993a.

McGregor, J. L., H. B. Gordon, I. G. Watterson, M. R. Dix, and L. D. Rotstayn, The CSIRO 9-level atmospheric general circulation model *Tech. Pap. 26*, 89 pp., CSIRO, Mordialloc, Australia, Div. of Atmos. Res., 1993b.

National Academy of Sciences (NAS) GCIP: Global Energy and Water Cycle Experiment (GEWEX) Continental-Scale International Project. A Review of progress and opportunities, 93 pp., Washington, D. C., 1998.

National Climatic Data Center (NCDC), Hourly precipitation data. *Tech. Data, TD-3240*, 21 pp., U.S. Dep. of Comm., Washington, D. C., 1990.

Nie, D., T. Demetriades-Shah, and E.T. Kanemasu, Surface energy fluxes on four slope sites during FIFE 1988, *J. Geophys. Res, 97*, 18,641-18,649, 1992a.

Nie, D., E.T. Kanemasu, L.J. Fritschen, H.L. Weaver, E.A. Smith, S.B. Verma, R.T. Field, W.P. Kustas., and J.B. Stewart, An intercomparison of surface energy flux measurement systems used during FIFE 1987, *J. Geophys. Res., 97*, 18,715-18,724, 1992b.

Peterson, T. C., and R. S. Vose, An overview of the Global Historical Climatology Network temperature database, *Bull. Am. Meteorol. Soc., 78*, 2837-2849, 1997.

Phillips, T. J., *Documentation of the AMIP Models on the World Wide Web*, 14 pp., Lawrence Livermore Natl. Lab., Livermore, Calif., 1995.

Pielke, R. A., et al., A comprehensive meteorological modeling system - RAMS, *Meteorol. Atmos. Phys., 49*, 69-91, 1992.

Roads, J. O., S.-C. Chen, M. Kanamitsu, and H. Juang, Surface water characteristics in the NCEP global spectral model and reanalysis, *J. Geophys. Res.*, this issue.

Sellers, P.J., F.G. Hall, G. Asrar, D E. Strebel, and R.E. Murphy, An overview of the First International Satellite Land Surface Climatology Project (ISLSCP) Field Experiment (FIFE), *J. Geophys. Res., 97*, 18,345-18,371, 1992.

Seth, A., and F. Giorgi, The effects of domain choice on summer precipitation simulation and sensitivity in a regional climate model, *J. Clim., 11*, 2698-2712, 1998.

Smith, E.A., et al., Area-averaged surface fluxes and their time-space variability over the FIFE experimental domain, *J. Geophys. Res,, 97*, 18,599-18,622, 1992.

Stensrud, D. J., Importance of low-level jets to climate: A review, *J. Clim, 9*, 1698-1711, 1996.

Takle, E.S., Project to Intercompare Regional Climate Simulations (PIRCS), Preliminary Workshop, 17-18 November 1994, *Bull. Am. Meteorol. Soc , 76*, 1625-1626, 1995.

Tiedtke, M., A comprehensive mass flux scheme for cumulus parameterization in large-scale models, *Mon Weather Rev., 117*, 1779-1800, 1989.

Trenberth, K. E., and C. J. Guillemot, Evaluation of the global atmospheric moisture budget as seen from analyses, *J. Clim., 9*, 2239-2254, 1995.

Trenberth, K.E., and C.J. Guillemot, Physical processes involved in the 1988 drought and 1993 floods in North America, *J. Clim., 9*, 1288-1298, 1996.

World Meteorological Organization (WMO), Report of the Eleventh Session of the CAS/JSC Working Group on Numerical Experimentation, Reading, England, 30 October - 3 November 1995, *WMO Rep.*, 43 pp., 1996.

C. J. Anderson, R. W. Arritt, W. J. Gutowski Jr., Z. Pan, R. Ramos da Silva, and E. S. Takle, Department of Agronomy, 3010 Agronomy, Iowa State University, Ames, IA 50011. (gstakle@iastate.edu)

D. Caya and R. Laprise, Universite du Quebec a Montreal, Montreal, P.O. Box 8888, Succ. "Centre-Ville", H3C 3P8, Canada.

S.-C. Chen and J. O. Roads, Scrips Instituion of Oceanography, La, Jolla, CA 92037.

F. Giorgi, The Abdus Salam International Centre for Theoretical Physics, Trieste, P.O. BOX 586, 34100 Trieste, Italy.

J. Hesselbjerg Christansen and P. Lopez, Danish Meteorological Institute, Lyngbyvej 100, DK-2100, Copenhagen, Denmark.

S.-Y. Hong and H.-M. Henry Juang, National Centers for Environmental Prediction, Camp Springs, MD 20031.

J. Katzfey and J. McGregor, Commonwealth Scientific and Industrial Research Organisation, Private Mail Bag No. 1, Aspendale, Victoria, 3195, Australia.

W. M. Lapenta, Marshall Space Flight Center, Huntsville, AL 35812.

G. E. Liston and A. Pielke, Sr., Department of Atmospheric Science, Colorado State University, Fort Collins, CO 80521.

(Received September 1, 1998; revised May 20, 1999; accepted May 20, 1999.)